A Reprint from

Stefan Hildebrandt
Hermann Karcher
Editors

Geometric Analysis and Nonlinear Partial Differential Equations

Springer

A reprint from: S. Hildebrandt / H. Karcher (Eds.),
Geometric Analysis and Nonlinear Partial Differential Equations,
Springer-Verlag Berlin Heidelberg New York, 2003.
ISBN 3-540-44051-8

On Generalized Mean Curvature Flow in Surface Processing

Ulrich Clarenz[1], Gerhard Dziuk[2], and Martin Rumpf[1]

[1] Institut für Mathematik, Gerhard-Mercator-Universität Duisburg, Lotharstraße 65, 47048 Duisburg, {clarenz, rumpf}@math.uni-duisburg.de
[2] Institut für angewandte Mathematik, Albert Ludwigs Universität Freiburg, Hermann-Herder-Straße 10, 79104 Freiburg, gerd@mathematik.uni-freiburg.de

1 Introduction

Geometric evolution problems for curves and surfaces and especially curvature flow problems are an exciting and already classical mathematical research field. They lead to interesting systems of nonlinear partial differential equations and allow the appropriate mathematical modeling of physical processes such as material interface propagation, fluid free boundary motion, crystal growth.

On the other hand, curves and surfaces are essential objects in computer aided geometric design and computer graphics. Here, issues are fairing, modeling, deformation, and motion. Constructive and more explicit approaches based for instance on splines are nowadays already classical tools. More recently geometric evolution problems and variational approaches have entered this research field as well and have turned out to be powerful tools. Their strength relies on the possibility to mathematically model problems on a continuous level, initially not worrying about the discretization. Furthermore, the resulting models come along with natural Galerkin discretizations which lead to consistent and simple algorithms mostly based on widespread simplicial grids approximating the continuous curves and surfaces [12, 26, 27, 36].

Not very surprisingly the resulting models mostly lead to similar geometric evolution problems as known from the above physical applications. Again systems of nonlinear partial differential equations control transport and diffusion phenomena in curve and surface processing applications.

Here, we will report on recent results concerning generalized mean curvature motion and its application in curve and surface fairing.

The processing of detailed triangulated surfaces is a fundamental topic in computer aided geometric design and in computer graphics. Nowadays, various such surfaces are delivered from different measurement techniques [9] or derived from two- or three dimensional data sets [28]. Recent laser scanning technology for example enables very fine triangulations of real world surfaces and sculptures. Also from medical image generation methods, such as CT and MRI devices or 3D ultrasound, certain surfaces of interest can be extracted - frequently in triangulated form - at a

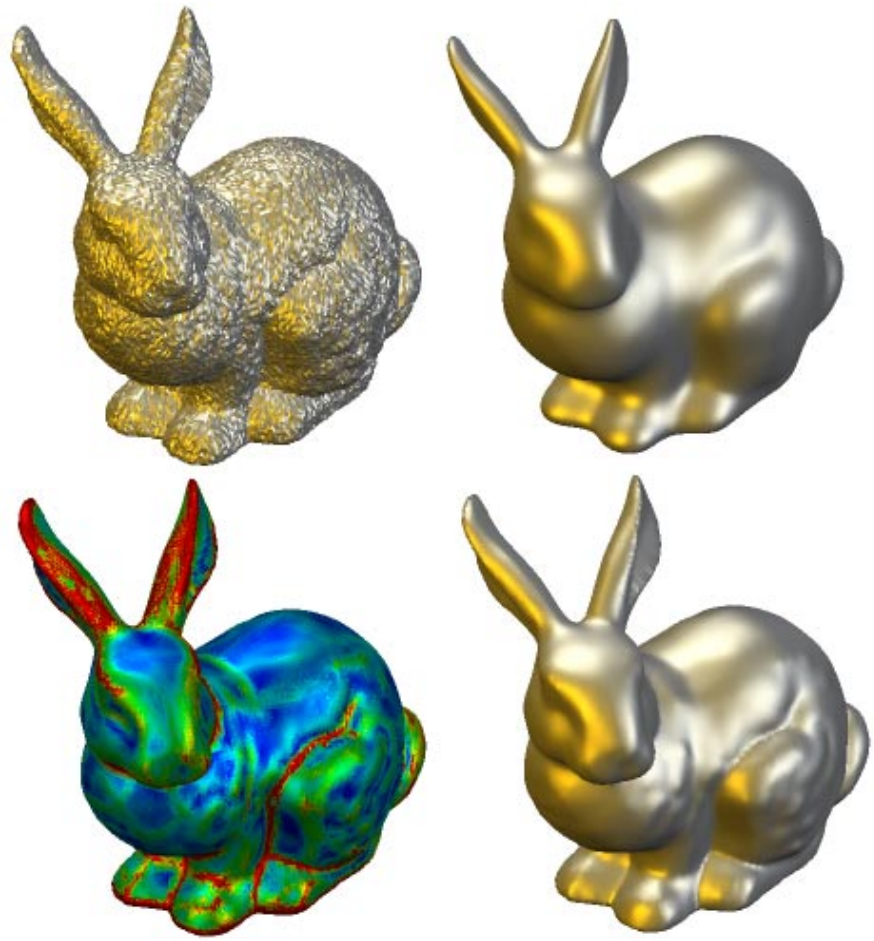

Fig. 1. *A noisy initial surface (top left) is evolved by discrete mean curvature flow (top right) and by the new anisotropic diffusion method (bottom right). Furthermore for the latter surface the dominant principal curvature - on which the diffusion tensor depends - is color coded (bottom left). The snapshots are taken at the same time-steps. (cf. color plate 8, Page 670)*

high resolution for further post processing and analysis. These surfaces are usually characterized by interesting features, such as edges and corners. On the other hand, they are typically disturbed by noise, which is often due to local measurement errors.

The aim of this paper is to discuss methods which allow the *fairing of discrete curves and surfaces*. Additionally they are able to *retain and even enhance important features such as surface edges and corners*. Figure 1 shows the performance of the basic method and compares it with a simple smoothing by mean curvature flow, the appropriate geometric "Gaussian" smoothing filter. Two alternative approaches are presented and compared:

– An anisotropic geometric diffusion problem is presented which respects edge features and in addition incorporates tangential smoothing along noisy edges.
– An anisotropic energy is formulated, where the local energy integrand reflects detected geometric features.

Both methods have in common that they are based on a local surface classification and the actual surface evolution which locally depends on the results of the classification. Furthermore they both lead to anisotropic curvature motion problems. A scale of successively smoothed representations is generated, where time is considered as the scale parameter. Such approaches have been originally developed for image processing purposes. Here we generalize them to curve and surface processing.

The methods differ with respect to the type of local classification and the model starting point. On the one hand, we model an anisotropic diffusion tensor in the geometric evolution problem. On the other hand, we define an energy density and ask for the gradient flow with respect to the corresponding energy. Furthermore, appropriate finite element algorithms based on the schemes in [15, 17] are proposed to discretize the continuous evolution problems. For convergence results in 1D we refer to [16, 17]. For 2D graphs in $\mathbb{R}^3$ an error analysis is contained in [11, 10].

The paper is organized as follows. First, in Section 2 we will discuss the background work on surface fairing by geometric smoothing and on image processing. In the following paragraph we collect some important notation. In Section 3 we introduce the different approaches to anisotropic curvature motion, i.e., the parabolic problem for an anisotropic Laplace Beltrami operator and the gradient flow for a spatially varying crystalline energy density. Their principal difference is discussed in Section 3.3. In Section 4 we derive finite element discretizations for both types of methods. Furthermore, in Section 5 the local classification types are introduced and in Section 6 the different classifications are incorporated in the geometric evolution approaches to steer the local evolution.

The volume enclosed by a surface without boundary is an important characteristic, which we should try to preserve during processing. Section 6 ends with a theorem that enables us to define generalized resp. anisotropic mean curvature motion keeping fixed the volume enclosed by the evolving surface.

2 Image and Surface Processing Background

In physics, diffusion is known as a process that equilibrates spatial variations in concentration. If we consider some initial noisy concentration or image intensity ρ_0 on a domain $\Omega \subset \mathbb{R}^2$ and seek solutions of the linear heat equation

$$\partial_t \rho - \Delta \rho = 0 \tag{1}$$

with initial data ρ_0 and natural boundary conditions on $\partial\Omega$, we obtain a scale of successively smoothed concentrations $\{\rho(t)\}_{t\in\mathbb{R}^+}$. For $\Omega = \mathbb{R}^2$ the solution of this parabolic problem coincides with the filtering of the initial data using a Gaussian filter $\overline{G}_\sigma^\infty(x) = (2\pi\sigma^2)^{-1} e^{-x^2/(2\sigma^2)}$ of width or standard deviation σ, i.e., $\rho(\sigma^2/2) =$

$\overline{G}_\sigma^\infty * \rho_0$. Concerning the smoothing of disturbed surface geometries one may ask for analogues strategies. The geometrical counterpart of the Euclidian Laplacian Δ on smooth surfaces is the Laplace Beltrami operator $\Delta_\mathcal{M}$ [14, 5]. Thus, one obtains the geometric diffusion $\partial_t x = \Delta_{\mathcal{M}(t)} x$ for the coordinates x on the corresponding family of surfaces $\mathcal{M}(t)$.
From differential geometry [13] we know that the mean-curvature vector hn equals the Laplace Beltrami operator applied to the immersion x of a surface $\mathcal{M}$:

$$h(x)n(x) = -\Delta_\mathcal{M} x. \tag{2}$$

Thus geometric diffusion is equivalent to mean curvature motion (MCM)

$$\partial_t x = -h(x)n(x)\ , \tag{3}$$

where $h(x)$ is the corresponding mean curvature (here defined as the sum of the two principal curvatures), and $n(x)$ is the normal on the surface at point x. In dimensions higher than two, singularities may occur in the evolution. Generalized - so called viscosity solutions - can be defined in terms of a level set formulation

$$\partial_t \phi - |\nabla\phi| \mathrm{div}\left(\frac{\nabla\phi}{|\nabla\phi|}\right) = 0\,.$$

Existence in this context has been proved by Evans and Spruck [18]. The mean curvature h is known to be the first variation of the surface area $\int_\mathcal{M} dA$. We obtain for the area $\mathrm{Ar}(\omega(t))$ of a subset $\omega(t)$ of a smooth surface $\mathcal{M}$ undergoing the MCM evolution (cf. [23]) $\frac{d}{dt}\mathrm{Ar}(\omega(t)) = -\int\limits_{\omega(t)} H^2 dA$. This is one indication for the strong regularizing effect of MCM.

In the context of Finsler geometry MCM can be generalized considering a 1-homogeneous convex scalar function $\gamma(\cdot)$ and a weighted area $\int_\mathcal{M} \gamma(N) dA$ depending on the surface orientation. As its first variation we obtain the weighted mean curvature h_γ [38, 6]. The corresponding anisotropic curvature flow has been studied for instance by Bellettini and Paolini [2].

On triangulated surfaces as they frequently appear in geometric modeling and computer graphics applications, several authors introduced discretized MCM operators [36, 26, 27, 22, 12]

Unfortunately MCM doesn't only decrease the geometric noise due to imprecise measurement but also smoothes out geometric features such as edges and corners of the surface. Hence, we seek models which improve a simple high pass filtering.

In image processing, Perona and Malik [31] proposed a nonlinear diffusion method, which modifies the diffusion coefficient at edges. Edges are indicated by steep intensity gradients. For a given initial image ρ_0 they considered the evolution problem

$$\partial_t \rho - \mathrm{div}\left(G\left(\frac{\|\nabla\rho\|}{\lambda}\right)\nabla\rho\right) = 0 \tag{4}$$

Fig. 2. *Isotropic Perona-Malik diffusion (right) is applied to a noisy initial image (left).*

for some parameter $\lambda \in \mathbb{R}^+$. For increasing time t - the scale parameter - the original image at the initial time is now successfully smoothed and image patterns are coarsened. But simultaneously edges are enhanced if one chooses a diffusion coefficient $G(.)$ which suppresses diffusion in areas of high gradients (cf. Fig. 2). A suitable choice for G is

$$G(s) = \left(1 + s^2\right)^{-1} . \tag{5}$$

Thus edges are classified by the involved parameter λ.

Kawohl and Kutev [24] gave a detailed analysis of the diffusion types in this method. Unfortunately the above original Perona and Malik model is still ill-posed because there is a true backward diffusion in areas of large gradients. Catté et al. [4] proposed a regularization method where the diffusion coefficient is no longer evaluated on the exact intensity gradient. Instead they suggested to consider the gradient evaluation on a prefiltered image.

Weickert [37] improved this method taking into account anisotropic diffusion, where the Perona Malik type diffusion is concentrated in one direction, for instance the gradient direction of a prefiltered image. This leads to an additional tangential smoothing along edges and amplifies intensity correlations along lines. Kimmel [25] generalized the scale space approach for planar images to the case of images mapped on surfaces.

Unfortunately, none of the above models is invariant under gray value transformations. In the axiomatic work by Alvarez et al. [1] general nonlinear evolution problems were derived from a set of axioms. Especially including the axiom of gray value invariance they end up with a curvature evolution model, i.e.,

$$\partial_t \phi - |\nabla \phi| \left(t \operatorname{div} \left(\frac{\nabla \phi}{|\nabla \phi|} \right) \right)^{\frac{1}{3}} = 0 .$$

Beyond this result, curvature motion based models proved as successful ingredients in segmentation and image enhancement methods. They have been considered by Pauwels et al. [30]. Sapiro [34] proposed a modification of MCM considering a diffusion coefficient which depends on the image gradient. Malladi and Sethian [29] presented a numerical level set method on 2D images called "min/max" flow which also considers the curvature evolution. In [7] and [32] anisotropic curvature motion methods on parametric surfaces (which will partially be revisited here) and on the entity of level sets of a 3D image have been considered. For an exposition and further references on geometric concepts in image processing we refer to the book of Sapiro [35].

Notation

Let us summarize notations and conventions we use in the sequel. We consider a parameter manifold $\mathcal{M}$ which essentially fixes the topological type of immersed surfaces $x : \mathcal{M} \to \mathbb{R}^{d+1}$. The parameter on $\mathcal{M}$ is denoted by ξ. For immersions x the differential Dx induces canonically a metric on $\mathcal{M}$ via the following relation which holds for all $v, w \in \mathcal{T}\mathcal{M}$

$$g(v, w) = Dx(v) \cdot Dx(w) \,.$$

The scalar product in $\mathbb{R}^m$ is denoted by $\cdot$. For smooth functions on $\mathcal{M}$ we can define a gradient $\nabla_{\mathcal{M}}$ or $\text{grad}_{\mathcal{M}}$ as the representation of its differential in the metric g, i.e.,

$$df(v) =: g(\nabla_{\mathcal{M}} f, v) = g(\text{grad}_{\mathcal{M}} f, v) \,,$$

for all $v \in \mathcal{T}\mathcal{M}$. The Levi-Civita connection will be denoted by ∇. With the Levi-Civita connection at hand we define the divergence of a vector field v by

$$\text{div}_{\mathcal{M}} v = \text{tr}\,(\nabla_{\bullet} v) \,,$$

which is nothing but the trace of the endomorphism $w \mapsto \nabla_w v$. This definition generalizes to the divergence of mappings $z : \mathcal{M} \to \mathbb{R}^{d+1}$ by:

$$\text{div}_{\mathcal{M}} z = \text{tr}\,\left(Dx^{-1}[Dz(\,\cdot\,)]^{tan}\right) \,,$$

where "^{tan}" represents the tangential component of Dz. For tangential mappings z, i.e., $z = Dx(v)$, with $v \in \mathcal{T}\mathcal{M}$ we have the identity $\text{div}_{\mathcal{M}} z = \text{div}_{\mathcal{M}} v$.

The manifolds $\mathcal{M}$ are assumed to be oriented and the normal mapping will be denoted by $n : \mathcal{M} \to S^d$, where d is the dimension of the manifold $\mathcal{M}$. This enables us to define the shape operator S by

$$g(S_{\mathcal{T}_x\mathcal{M}} w, v) := \partial_w N \cdot Dx(v) \,.$$

The trace of the shape operator is the classical mean curvature $h = \text{tr}\; S_{\mathcal{T}_x\mathcal{M}}$. We often write $S = S_{\mathcal{T}_x\mathcal{M}}$ if a misunderstanding is ruled out.

The Laplacian $\operatorname{div}_{\mathcal{M}} \nabla_M$ is denoted by $\Delta_{\mathcal{M}}$. We will use the concept of tangential gradients. The tangential gradient for a function $u \in C^1(\mathbb{R}^{d+1})$ is defined as

$$\underline{D}u = \nabla_{\mathbb{R}^{d+1}} u - (n \cdot \nabla_{\mathbb{R}^{d+1}} u)\, n\,.$$

For the components of $\underline{D}u$ we have $\underline{D}_i u = dx_i(\nabla_{\mathcal{M}} u)$. We sometimes identify $x(\mathcal{M})$ and $\mathcal{M}$ and in this sense $\underline{D}u = \nabla_{\mathcal{M}} u$. Note the relation for the Laplacian $\Delta_{\mathcal{M}} u = \sum_i \underline{D}_i \underline{D}_i u$. For more details on tangential gradients we refer to [21, Chapter 16]. Integration over $\mathcal{M}$ leads to the L^2-scalar product of L^2-functions f, g on $\mathcal{M}$:

$$(f, g) := \int_{\mathcal{M}} f \cdot g \, dA\,.$$

Finally, let us from now on use Einstein summation convention.

3 Anisotropic Curvature Motion

3.1 Generalized Mean Curvature Motion

Let $x : \mathcal{M} \to \mathbb{R}^{d+1}$, $\mathcal{M}$ an orientable manifold of dimension d, be an immersion with normal $n : \mathcal{M} \to S^d$. In this section we consider general endomorphisms of the tangent space

$$a : \mathcal{T}\mathcal{M} \to \mathcal{T}\mathcal{M}$$

and the corresponding generalized mean curvature flow:

$$\partial_t x = -h_a n, \quad h_a = \operatorname{tr}(a \circ S)\,, \tag{6}$$

where S denotes the shape operator. The variational formulation of this problem is:

$$(\partial_t x, \vartheta) = -\int_{\mathcal{M}} h_a \, (n \cdot \vartheta)\, dA$$

for all $\vartheta \in C_0^1(\mathcal{M}, \mathbb{R}^{d+1})$. In case of classical mean curvature h, the relation $\Delta_{\mathcal{M}} x = -hn$ leads to a re-formulation of the above equation:

$$(\partial_t x, \vartheta) = \int_{\mathcal{M}} \Delta_{\mathcal{M}} x \cdot \vartheta \, dA = -\int_{\mathcal{M}} g(\nabla_{\mathcal{M}} x, \nabla_{\mathcal{M}} \vartheta) dA.$$

Let us already emphasize that this formulation will enable the later discretization by finite elements (cf. [15]). Now, we seek a generalization of the equation $\Delta_{\mathcal{M}} x = -hn$ that involves generalized mean curvatures. The next theorem gives such a generalization. The idea is to make use of the operator $\Delta_a \cdot = \operatorname{div}_{\mathcal{M}}(a \nabla_{\mathcal{M}} \cdot)$. We will see that the application of this operator to x leads to tangential components which are given by the divergence of the endomorphism a. For this reason we remind of the definition and basic properties of the divergence:

Definition 3.1 *The divergence of an endomorphism*

$$a : \mathcal{TM} \to \mathcal{TM}$$

is a vector field given by

$$g(\mathrm{div}_{\mathcal{M}} a, v) := \mathrm{tr}(\nabla_{\bullet} a^* v),$$

where the above equation is supposed to hold for all $v \in \mathcal{TM}$.

From this definition we obtain the representation:

$$\begin{aligned} g(\mathrm{div}_{\mathcal{M}} a, v) &= g(\nabla_{e_i} a^* v, e_i) \\ &= g(v, \nabla_{e_i} a\, e_i) \end{aligned}$$

and thus $\mathrm{div}_{\mathcal{M}} a = \nabla_{e_i} a\, e_i$ for an orthonormal basis $\{e_1, \dots, e_d\} \subset \mathcal{T}_\xi \mathcal{M}$. Hence we obtain in coordinates

$$\mathrm{div}_{\mathcal{M}} a = g^{ij} \nabla_{\frac{\partial}{\partial \xi_i}} a \, \frac{\partial}{\partial \xi_i}.$$

Now we are prepared to formulate

Theorem 3.2 *Let* $x : \mathcal{M} \to \mathbb{R}^{d+1}$ *be an immersion of an orientable* d*-dimensional manifold. If* $a : \mathcal{TM} \to \mathcal{TM}$ *is differentiable, linear and symmetric on each tangent space, then there is a second order differential operator* Θ_a *with*

$$\Theta_a x = -h_a n,$$

where $h_a = \mathrm{tr}\,(a \circ S)$. *The second order operator is given by*

$$\Theta_a(\cdot) = \Delta_a(\cdot) - (\mathrm{div}_{\mathcal{M}} a)(\cdot)\,.$$

A proof of the above theorem can be found in [6]. It shows that we are able to express the velocity $-h_a n$ via projection of $\mathrm{div}_{\mathcal{M}}(a\, \nabla_{\mathcal{M}} x)$ onto the space spanned by the normal n. Consequently, the equation $\partial_t x = -h_a n$ can be written as follows:

$$\begin{aligned} v &= \mathrm{div}_{\mathcal{M}}(a\, \nabla_{\mathcal{M}} x) \\ \partial_t x &= (v \cdot n)\, n\,. \end{aligned} \tag{7}$$

Once more, let us emphasize that this formulation with the operator in divergence form enables us to generalize the algorithm in [15] for mean curvature motion (see sections 4 and 6.1).

3.2 Anisotropic Energies and Gradient Flow

As it is well known mean curvature evolution $\partial_t x = -hn$ can be considered as L^2-gradient flow w.r.t. the area functional. In this section we study more generally, so called anisotropic energies. Here the functional $\int_{\mathcal{M}} dA$ is generalized to the energy

$$E_\gamma[x] = \int_{\mathcal{M}} \gamma(\xi, n(\xi))\, dA(\xi)\,, \tag{8}$$

where

$$\begin{aligned} \gamma : \mathcal{M} \times \mathbb{R}^{d+1} &\longrightarrow \mathbb{R}^+ \\ (\xi, z) &\longmapsto \gamma(\xi, z) \end{aligned} \tag{9}$$

is an integrand of class $C^2(\mathcal{M} \times (\mathbb{R}^{d+1} - \{0\}))$ which is positively homogeneous of degree 1 in the z-variable.

The corresponding functional not only depends on the normal mapping of x but also on the parameter ξ. Thus favorable normal directions w.r.t. the energy E_γ may differ locally.

The derivative of E involves the generalized mean curvature $h_\gamma = \operatorname{tr}(a_\gamma \circ S)$ induced by γ, where

$$\begin{aligned} a_\gamma : \mathcal{TM} &\to \mathcal{TM} \\ (\xi, v) &\mapsto (\xi, Dx^{-1} \circ D_z^2\gamma(\xi, n(\xi)) \circ Dx(v)). \end{aligned}$$

The endomorphism $D_z^2\gamma(\xi, n(\xi)) : \mathbb{R}^{d+1} \to \mathbb{R}^{d+1}$ can be interpreted as an endomorphism on the orthogonal complement $n(\xi)^\perp$ of n. Indeed – due to the homogeneity of γ – we have

$$D_z^2\gamma(\xi, n)n = 0$$

and therefore, a_γ is well defined. The application of the derivative of E_γ to $\vartheta \in C_0^1(\mathcal{M}, \mathbb{R}^{d+1})$ is given by

$$\langle E'_\gamma[x], \vartheta \rangle = \int_{\mathcal{M}} h_\gamma(\vartheta \cdot n)\, dA.$$

For more details and proofs we refer to [6], [33], [38]. The gradient flow corresponding to E_γ is

$$\partial_t x = -h_\gamma n\,.$$

Wulff-Shape and Frank-Diagram

Let us restrict for a moment to the case, that γ is constant w.r.t. the ξ-variable, i.e., $\gamma(\xi, z) = \gamma(z)$. In the following we will explain that there is a bijection between convex bodies and these anisotropic integrands resp. energies. For the visualization of the energy E_γ one frequently uses the so called Wulff-shape and Frank-diagram. First let us consider a compact convex body $\mathcal{K} \subset \mathbb{R}^d$. Then we have

Proposition 3.3 *There is a 1-homogeneous and convex function $\gamma : \mathbb{R}^d \to \mathbb{R}$, called the support function of the compact convex body $\mathcal{K}$, such that*

$$\mathcal{K} = \{x \in \mathbb{R}^d \mid x \cdot \nu \le \gamma(\nu) \text{ for all } \nu \in \mathbb{R}^d\}\,.$$

Conversely, the set $\mathcal{K}$ defined by the above relation is convex if γ is convex and 1-homogeneous. In case $\gamma(\nu) > 0$ for $\nu \neq 0$, the origin is contained in int $\mathcal{K}$.

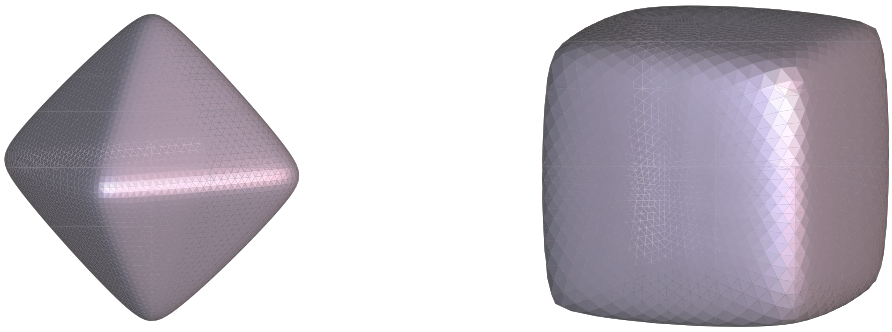

Fig. 3. A typical example of a Wulff-shape and the corresponding Frank-diagram

The above proposition shows a bijective relation between convex bodies and convex 1-homogeneous functions. A proof can be found in the classical introduction to convex analysis [3].

Now we fix an integrand γ of an energy E. The corresponding convex body $\mathcal{K}$ will be denoted by $\mathcal{W}_\gamma$ and is called Wulff-shape. (This denomination goes back to the work [39] of the cristallograph G. Wulff from 1901.) Introducing the dual γ^* of γ which is given by

$$\gamma^*(z^*) = \sup_{z \in S^{d-1}} \frac{z \cdot z^*}{\gamma(z)} \,,$$

$\mathcal{W}_\gamma$ can be described in a different way:

$$\mathcal{W}_\gamma = \{x \in \mathbb{R}^d \,|\, \gamma^*(x) \leq 1\} \,.$$

The justification of the name *dual* is the content of the next

Proposition 3.4 *Let $\gamma : \mathbb{R}^d \to \mathbb{R}^+$ be a convex integrand then the duality relation $\gamma^{**} := (\gamma^*)^* = \gamma$ holds.*

For a proof of this proposition we refer to [2]. The dual shape $\mathcal{F}_\gamma$ of the Wulff-shape $\mathcal{W}_\gamma$ is according to Proposition 3.4 given by

$$\mathcal{F}_\gamma = \{z \in \mathbb{R}^d \,|\, \gamma(z) \leq 1\}$$

and is called the Frank diagram.

Example 3.5 *Consider the integrand in $\mathbb{R}^d$:*

$$\gamma_p(z) = \left(\sum_i |z_i|^p \right)^{\frac{1}{p}} \,, \quad p \in [1, \infty] \,,$$

then the dual integrand is given by

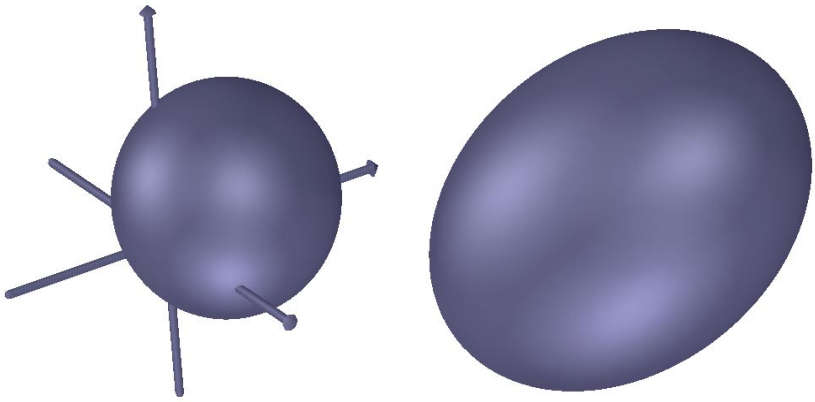

Fig. 4. Here, the Wulff shape is a sphere whose center is not the origin.

$$\gamma_p^*(z^*) = \left(\sum_i |z_i^*|^{p^*} \right)^{\frac{1}{p^*}} = \gamma_{p^*}(z^*),$$

where $\frac{1}{p} + \frac{1}{p^*} = 1$.

Remark 3.6 *For the computation of Frank diagrams we derive a simple algorithm. Given a convex body with boundary* $\partial \mathcal{W}_\gamma$ *we would like to determine the boundary* $\partial \mathcal{F}_\gamma$ *of the corresponding Frank diagram. To this aim consider a point* ν *of the surface and the normal* n *in* ν*. The support function* γ *of the convex body evaluated in* $\frac{n}{n \cdot \nu}$ *equals 1. Therefore we consider the map* $f : \partial \mathcal{W}_\gamma \to \mathbb{R}^d$

$$f(\nu) = \frac{n}{n \cdot \nu}$$

and we have $\gamma(f(\nu)) = 1$.

Wulff-shapes are known to be the solution of an isoperimetric problem. The boundary of $\mathcal{W}_\gamma$ is the minimizer of E_γ in the class of surfaces enclosing the same volume. For details we refer to [19] and [20].

3.3 Comparing the Two Approaches

The preceding section contained two methods to define generalized resp. anisotropic mean curvature motion.

The generalized mean curvature approach consists in introducing an anisotropic tensor $a : \mathcal{TM} \to \mathcal{TM}$, without specifying this tensor in detail. In this sense one might think of $a = a(\xi)$ depending on the parameter $\xi \in \mathcal{M}$.

On the other hand, we considered a gradient flow defined by the energy $E_\gamma[x] = \int_{\mathcal{M}} \gamma(\xi, n(\xi))\, dA$. Principally, this flow is nothing but a special case of a generalized mean curvature flow choosing $a(\xi) = Dx^{-1} D_z^2 \gamma(\xi, n(\xi)) Dx$. We point at the fact that for this special choice the tensor a depends on the geometry of x via the surface normal n.

4 Discretization

4.1 Generalized Mean Curvature

Using the operator Θ_a we can give a weak formulation of (6), which can numerically be solved by finite elements:

$$\int_{\mathcal{M}} \partial_t x \cdot \vartheta \; dA = \int_{\mathcal{M}} \Theta_a x \cdot \vartheta \; dA.$$

Concerning numerical realization of the Θ_a-operator we emphasis that the tangential term $\mathrm{div}_{\mathcal{M}} a$ has to be taken into consideration. Otherwise, on a triangulated surface one observes strong tangential shifts leading to irregular meshes. The operator $\mathrm{div}_{\mathcal{M}} a$ is not easy to handle numerically. Therefore we use a projection of the Δ_a-operator as follows:

$$\Theta_a x = (\Delta_a x \cdot n) n.$$

Let us identify from now on $\mathcal{M}$ and $x(\mathcal{M})$. Furthermore, for time discretization, we follow [15] and view in each time-step $x^{(k+1)}$ as a mapping from $\mathcal{M}^{(k)}$ onto $\mathcal{M}^{(k+1)}$ instead of a mapping defined on a fixed parameter domain. For a semi-implicit time discretization of (7) we are lead to:

$$\int_{\mathcal{M}^{(k)}} v^{(k+1)} \cdot \vartheta \, dA = \int_{\mathcal{M}^{(k)}} g\left(a^{(k)} \nabla_{\mathcal{M}^{(k)}}(x^{(k)} + \tau v^{(k+1)}), \nabla_{\mathcal{M}^{(k)}} \vartheta\right) dA$$

for $\vartheta \in C_0^1(\mathcal{M})$ and

$$x^{(k+1)} = x^{(k)} + \tau \left(v^{(k+1)} \cdot n^{(k)}\right) n^{(k)}.$$

This scheme defines approximations $x^{(k)}$ of $x(\tau k)$.

Next, we discuss the spatial discretization. To clarify the notation we will always denote discrete quantities with upper case letters to distinguish them from the corresponding continuous quantities in lower case letters.

We restrict our considerations to the case $d = 2$ and consider a polyhedron consisting of triangles $\mathcal{M}_h$ which is an approximation of $\mathcal{M}$. X will be the parametrization of $\mathcal{M}_h$, i.e., X is in each component an affine linear function on the triangles of $\mathcal{M}_h$. The corresponding finite element space

$$\mathcal{V}_h = \{\Phi \in C^0(\mathcal{M}_h) \;\big|\; \Phi_T \in \mathcal{P}_1, T \in \mathcal{M}_h\} \tag{10}$$

consisting of those functions being affine linear on each triangle of $\mathcal{M}_h$ has the basis $\{\Phi_j\}_{j=1}^J$, where J is the number of vertices of $\mathcal{M}_h$ and $\Phi_j(X_i) = \delta_{ij}$ for all vertices X_i. We can represent X as

$$X = \overline{X}_j \Phi_j,$$

i.e., $X \in [\mathcal{V}_h]^3$. The discretization of $a : \mathcal{TM} \to \mathcal{TM}$ will be denoted by A and will be considered as constant symmetric positive definite endomorphism of $\mathbb{R}^3$ on each triangle.

The gradient-operator on $\mathcal{M}_h$ is now $\nabla_{\mathcal{M}_h}$, the gradient on the Lipschitz surface $\mathcal{M}_h$ (see [15] for more details). For the fully discrete semi implicit scheme we introduce the discrete velocities $V^{(k)} \in [V_h]^3$ and obtain for all $\Phi \in \mathcal{V}_h$:

$$\int_{\mathcal{M}_h^{(k)}} V^{(k+1)} \cdot \Phi = \int_{\mathcal{M}_h^{(k)}} \left(A^{(k)} \nabla_{\mathcal{M}_h^{(k)}} (X^{(k)} + \tau V^{(k+1)}) \cdot \nabla_{\mathcal{M}_h^{(k)}} \Phi \right),$$

$$X^{(k+1)} = X^{(k)} + \tau (V^{(k+1)} \cdot N^{(k)}) N^{(k)},$$

where $N^{(k)}$ is given on each vertex $\overline{X}_j$ by the weighted sum $N_j^{(k)} = \frac{\sum_{i=1}^{\ell_j} |T_i| N_{T_i}^{(k)}}{\left| \sum_{i=1}^{\ell_j} |T_i| N_{T_i}^{(k)} \right|}$ and $N_{T_i}^{(k)}$ is the normal on $T_i \in \mathcal{M}_h$ with $\overline{X}_j \in \overline{T}_i$. Here ℓ_j is the number of elements T_i with node $\overline{X}_j$. Thus starting with $\mathcal{M}_h^{(0)}$ we obtain a sequence of triangulated surfaces $\mathcal{M}_h^{(k)}$ approximating $\mathcal{M}(t)$ at time $t = k\tau$. The implementation of this discrete scheme is straightforward. We introduce the mass matrix $M^{(k)}$ and the stiffness matrix $L^{(k)}$:

$$M_{ij}^{(k)} = \int_{\mathcal{M}_h^{(k)}} \Phi_i \Phi_j \, dA, \quad L_{ij}^{(k)} = \int_{\mathcal{M}_h^{(k)}} \left(A^{(k)} \nabla_{\mathcal{M}_h^{(k)}} \Phi_i \right) \cdot \nabla_{\mathcal{M}_h^{(k)}} \Phi_j \, dA$$

The computation of $V^{(k+1)}$ requires the solution of the linear systems

$$(M^{(k)} - \tau L^{(k)}) \overline{V}_l^{(k+1)} = L^{(k)} \overline{X}_l^{(k)}, \tag{11}$$

where we set $\overline{V}_l^{(k+1)} = (\overline{V}_{1,l}^{(k+1)}, \ldots, \overline{V}_{J,l}^{(k+1)})$ and $\overline{X}_l^{(k+1)} \in \mathbb{R}^J$ analogue. For more details we refer to [7].

The above algorithm is clearly applicable for the case $d = 1$. Let us have a look at this simple case only considering spatial discretization. The system we have to solve is:

$$\int_{\mathcal{M}_h(t)} \langle V_h, \Phi_k \rangle + \int_{\mathcal{M}_h(t)} \langle A \nabla_{\mathcal{M}_h} X_h, \nabla_{\mathcal{M}_h} \Phi_k \rangle = 0$$

$$\partial_t X_h = \langle V_h, N_h \rangle N_h$$

4.2 Anisotropic Gradient Flow

The 1D case.
In this section we want to derive a numerical scheme for energies as defined in (8) in case of curves, thus $\mathcal{M} = S^1$. The algorithm we derive here is related to [17]. Our starting point for the computation of the generalized mean curvature flow

$$\partial_t x = -h_\gamma n$$

is the weak formulation

$$\int_{S^1} x_t \vartheta \, |x_\xi| d\xi + \int_{S^1} \gamma_z(\xi, x_\xi^\perp) \vartheta_\xi^\perp d\xi = 0 \;\text{ for all }\; \vartheta \in C^1(S^1, \mathbb{R}^2)\,. \tag{12}$$

The symbol $^\perp$ denotes a rotation by 90^o. For the spatial discretization of this weak form of curvature flow consider a decomposition of $S^1 = \mathbb{R}/2\pi$ into intervals:

$$[0, 2\pi] = \bigcup_{j=1}^{J} I_j, \quad I_j = [\xi_{j-1}, \xi_j], \quad h_j = |I_j|.$$

The underlying finite element space is $[\mathcal{S}_h]^2$, where

$$\mathcal{S}_h = \{\Phi \in C^0(S^1) \,|\, \Phi_{|I_j} \in \mathcal{P}_1,\, j = 1, \ldots, J\}$$

The discrete solution $X : (0, T) \to [\mathcal{S}_h]^2$ is represented as:

$$X(t, \xi) := \overline{X}_j(t) \Phi_j(\xi).$$

Now we assume γ to be a piece-wise linear function for fixed $z \in S^1$, i.e.,

$$\gamma(\xi, z) = \Phi_j(\xi) \gamma_j(z).$$

A discrete solution X fulfills

$$\int_{S^1} \partial_t X |X_\xi| \Phi d\xi + \int_{S^1} \gamma_z(\xi, X_\xi^\perp) \Phi_\xi^\perp d\xi = 0 \;\text{ for all }\; \Phi \in [\mathcal{S}_h]^2.$$

Taking $\Phi = \Phi_j \in \mathcal{S}_h$ separately for each component as test function one obtains:

$$\int_{S^1} \gamma_z^\perp(\xi, X_\xi^\perp) \Phi_{j,\xi} d\xi =$$

$$\frac{1}{2}\left[\gamma_{j-1,z}^\perp (\overline{X}_j^\perp - \overline{X}_{j-1}^\perp) + \gamma_{j,z}^\perp (\overline{X}_j^\perp - \overline{X}_{j-1}^\perp)\right]$$

$$-\frac{1}{2}\left[\gamma_{j,z}^\perp (\overline{X}_{j+1}^\perp - \overline{X}_j^\perp) + \gamma_{j+1,z}^\perp (\overline{X}_{j+1}^\perp - \overline{X}_j^\perp)\right]$$

Lumping of masses leads to:

$$\frac{1}{2}\partial_t \overline{X}_j(|\overline{X}_j - \overline{X}_{j-1}| + |\overline{X}_{j+1} - \overline{X}_j|)$$

$$-\frac{1}{2}\left[\gamma^{\perp}_{j-1,z}(\overline{X}^{\perp}_j - \overline{X}^{\perp}_{j-1}) + \gamma^{\perp}_{i,z}(\overline{X}^{\perp}_j - \overline{X}^{\perp}_{j-1})\right]$$

$$+\frac{1}{2}\left[\gamma^{\perp}_{j,z}(\overline{X}^{\perp}_{j+1} - \overline{X}^{\perp}_j) + \gamma^{\perp}_{j+1,z}(\overline{X}^{\perp}_{j+1} - \overline{X}^{\perp}_j)\right] = 0.$$

Introducing $q_j = |\overline{X}_j - \overline{X}_{j-1}|, \tau_j = (\overline{X}_j - \overline{X}_{j-1})/q_j$, $N_j = \tau_j^{\perp}$ and using the zero homogeneity of $\gamma_{j,z}$ in the z-variable we can rewrite the above equation as:

$$\begin{aligned} &\partial_t \overline{X}_j(q_j + q_{j+1}) - \gamma^{\perp}_{j-1,z}(N_j) \\ &- \gamma^{\perp}_{j,z}(N_j) + \gamma^{\perp}_{j,z}(N_{j+1}) + \gamma^{\perp}_{j+1,z}(N_{j+1}) = 0 \end{aligned} \tag{13}$$

For all i, j the following relation is valid:

$$\begin{aligned} \gamma^{\perp}_{j,z}(N_i) &= (\gamma^{\perp}_{j,z}(N_i) \cdot \tau_i)\tau_i + (\gamma^{\perp}_{j,z}(N_i) \cdot N_i)N_i \\ &= -(\gamma_{j,z}(N_i) \cdot N_i)\tau_i + (\gamma_{j,z}(N_i) \cdot \tau_i)N_i \\ &= -\gamma_j(N_i)\tau_i + (\gamma_{j,z}(N_i) \cdot \tau_i)N_i. \end{aligned}$$

Equation (13) now can be formulated as:

$$\begin{aligned} \partial_t \overline{X}_j(q_j + q_{j+1}) &+ \gamma_{j-1}(N_j)\tau_j + \gamma_j(N_j)\tau_j \\ &- \gamma_j(N_{j+1})\tau_{j+1} - \gamma_{j+1}(N_{j+1})\tau_{j+1} = \\ &\quad (\gamma_{j-1,z}(N_j) \cdot \tau_j)N_j + (\gamma_{j,z}(N_j) \cdot \tau_j)N_j \\ &- (\gamma_{j,z}(N_{j+1}) \cdot \tau_{j+1})N_{j+1} - (\gamma_{j+1}(N_{j+1}) \cdot \tau_{j+1})N_{j+1} \end{aligned}$$

and with $g_{i,j} = \gamma_i(N_j), g'_{i,j} = \gamma_{i,z}(N_j)\tau_j$ this leads to:

$$
\begin{aligned}
\partial_t \overline{X}_j (q_j + q_{j+1}) &- \left(\frac{g_{j-1,j}}{q_j} + \frac{g_{j,j}}{q_j} \right) \overline{X}_{j-1} \\
&+ \left(\frac{g_{j-1,j}}{q_j} + \frac{g_{j,j}}{q_j} + \frac{g_{j,j+1}}{q_{j+1}} + \frac{g_{j+1,j+1}}{q_{j+1}} \right) \overline{X}_j \\
&- \left(\frac{g_{j,j+1}}{q_{j+1}} + \frac{g_{j+1,j+1}}{q_{j+1}} \right) \overline{X}_{j+1} \\
&+ \left(\frac{g'_{j-1,j}}{q_j} + \frac{g'_{j,j}}{q_j} \right) \overline{X}^{\perp}_{j-1} \\
&- \left(\frac{g'_{j-1,j}}{q_j} + \frac{g'_{j,j}}{q_j} + \frac{g'_{j,j+1}}{q_{j+1}} + \frac{g'_{j+1,j+1}}{q_{j+1}} \right) \overline{X}^{\perp}_{j} \\
&+ \left(\frac{g'_{j,j+1}}{q_{j+1}} + \frac{g'_{j+1,j+1}}{q_{j+1}} \right) \overline{X}^{\perp}_{j+1} = 0
\end{aligned}
$$

We would like emphasize that this scheme is intrinsic, in the sense that it is independent of the parametrization. For the time-discretization we use a semi-implicit scheme, where q_j, $g_{i,j}$ and $g'_{i,j}$ are treated explicitly. For more details see [17].

The 2D case.
In the following we describe the discretization of the generalized mean curvature flow for anisotropic energies (8) depending only on the surface normal. The discretization will be such that it only contains the first derivatives of the anisotropy function γ. In abstract form the problem reads

$$
(\partial_t x, \vartheta) = -\langle E'_\gamma[x], \vartheta \rangle \tag{14}
$$

for every test function $\vartheta \in C^1_0(\mathcal{M}, \mathbb{R}^{d+1})$. For practical reasons we use the concept of tangential gradients for a reformulation of (14). Easy calculations show, that

$$
\begin{aligned}
\langle E'_\gamma[x], \vartheta \rangle &= \int_{\mathcal{M}} h_\gamma \, n \cdot \vartheta \, dA = \int_{\mathcal{M}} \operatorname{tr} \left(D^2_z \gamma(n) \, \nabla_{\mathcal{M}} n \right) \, n \cdot \vartheta \, dA \\
&= \int_{\mathcal{M}} \sum_{k,l=1}^{d+1} \gamma_{z_k z_l}(n) \, \underline{D}_k n_l \, n \cdot \vartheta \, dA \\
&= - \int_{\mathcal{M}} \sum_{k,l=1}^{d+1} \underline{D}_k \left(\gamma(n) \, \underline{D}_k x_l - \sum_{m=1}^{d+1} \gamma_{z_m}(n) \, n_l \, \underline{D}_k x_m \right) \vartheta_l \, dA \\
&= \int_{\mathcal{M}} \sum_{k,l=1}^{d+1} \left(\gamma(n) \, \underline{D}_k x_l \, \underline{D}_k \vartheta_l - \sum_{m=1}^{d+1} \gamma_{z_m}(n) \, n_l \, \underline{D}_k x_m \, \underline{D}_k \vartheta_l \right) dA \\
&= \int_{\mathcal{M}} \gamma(n) \, \nabla_{\mathcal{M}} x \cdot \nabla_{\mathcal{M}} \vartheta - \sum_{k,l=1}^{d+1} \gamma_{z_k}(n) \, n_l \, \nabla_{\mathcal{M}} x_k \cdot \nabla_{\mathcal{M}} \vartheta_l \, dA.
\end{aligned}
$$

Thus anisotropic mean curvature flow (14) can be written as

$$\int_{\mathcal{M}} \partial_t x \cdot \vartheta + \int_{\mathcal{M}} \gamma(n) \nabla_{\mathcal{M}} x \cdot \nabla_{\mathcal{M}} \vartheta \, dA \tag{15}$$
$$= \int_{\mathcal{M}} \sum_{k,l=1}^{d+1} \gamma_{z_k}(n) n_l \nabla_{\mathcal{M}} x_k \cdot \nabla_{\mathcal{M}} \vartheta_l \, dA.$$

for every $\vartheta \in C_0^1(\mathcal{M}, \mathbb{R}^{d+1})$. The right hand side of (15) can be simplified using the relation

$$\underline{D}_j x_k = \delta_{jk} - n_j n_k.$$

Hence

$$\int_{\mathcal{M}} \sum_{k,l=1}^{d+1} \gamma_{z_k}(n)\, n_l\, \nabla_{\mathcal{M}} x_k \cdot \nabla_{\mathcal{M}} \vartheta_l \, dA = \int_{\mathcal{M}} \sum_{k,l=1}^{d+1} \gamma_{z_k}(n)\, n_l\, \underline{D}_k \vartheta_l \, dA.$$

But as we shall see, the right hand side in (15) is numerically more convenient after time discretization. For isotropic mean curvature flow, i. e. for $\gamma(z) = |z|$, this right hand side vanishes. We also observe that the left hand side of (15) decouples with respect to the components of x.

For the discretization we restrict ourselves to $d = 2$. We use the following time discretization:

$$\int_{\mathcal{M}^{(k)}} \frac{1}{\tau} \left(x^{(k+1)} - x^{(k)} \right) \cdot \vartheta \, dA +$$
$$\int_{\mathcal{M}^{(k)}} \gamma(n^{(k)})\, \nabla_{\mathcal{M}^{(k)}} x^{(k+1)} \cdot \nabla_{\mathcal{M}^{(k)}} \vartheta \, dA$$
$$= \sum_{l,m=1}^{d+1} \int_{\mathcal{M}^{(k)}} \gamma_{z_m}(n^{(k)})\, n_l^{(k)}\, \nabla_{\mathcal{M}^{(k)}} x_m^{(k)} \cdot \nabla_{\mathcal{M}^{(k)}} \vartheta_l \, dA. \tag{16}$$

Here τ is the time step and $g^{(k)}$ stands for the evaluation of a generic function g on the k–th time level. $x^{(0)}$ is given by the initial surface.

The discretization in space is based on piece-wise linear finite elements similar to the approach above in Section 4.1.

We compute a sequence of time step solutions $X^{(k)}$ for $k = 0, \cdots$, where the initial polyhedron $X^{(0)}$ is the interpolant of $x^{(0)}$. The fully discrete scheme then reads: for every $\Phi \in [\mathcal{V}_h]^3$

$$\int_{\mathcal{M}_h^{(k)}} \frac{1}{\tau}\left(X^{(k+1)} - X^{(k)}\right)\cdot \Phi\, dA + \int_{\mathcal{M}_h^{(k)}} \gamma(N^{(k)})\, \nabla_{\mathcal{M}_h^{(k)}} X^{(k+1)} \cdot \nabla_{\mathcal{M}_h^{(k)}} \Phi\, dA = \sum_{l,m=1}^{3} \int_{\mathcal{M}_h^{(k)}} \gamma_{z_m}(N^{(k)})\, N_l^{(k)}\, \nabla_{\mathcal{M}_h^{(k)}} X_m^{(k)} \cdot \nabla_{\mathcal{M}_h^{(k)}} \Phi_l\, dA. \tag{17}$$

This linear system of equations is quite easy to implement. For given $\mathcal{M}_h^{(k)}$ we define the mass matrix $M^{(k)}$ as in Section 4.1, the stiffness matrix $L^{(k)}$ by

$$L_{ij}^{(k)} = \int_{\mathcal{M}_h^{(k)}} \gamma(N^{(k)}) \nabla_{\mathcal{M}_h^{(k)}} \Phi_i \cdot \nabla_{\mathcal{M}_h^{(k)}} \Phi_j\, dA$$

$(i, j = 1, \ldots, J)$, and the right hand sides $C_l^{(k)}$ by

$$C_{l,j}^{(k)} = \sum_{m=1}^{3} \int_{\mathcal{M}_h^{(k)}} \gamma_{z_m}(N^{(k)})\, N_l^{(k)}\, \nabla_{\mathcal{M}_h^{(k)}} X_m^{(k)} \cdot \nabla_{\mathcal{M}_h^{(k)}} \Phi_j\, dA$$

$(l = 1, 2, 3, j = 1, \ldots, J)$. In every time step of the scheme we have to solve 3 linear systems with the same matrix for the computation of $\overline{X}_l^{(k+1)} \in \mathbb{R}^J$:

$$\left(\frac{1}{\tau} M^{(k)} + L^{(k)}\right) \overline{X}_l^{(k+1)} = \frac{1}{\tau} L^{(k)} \overline{X}_l^{(k)} + C_l^{(k)}.$$

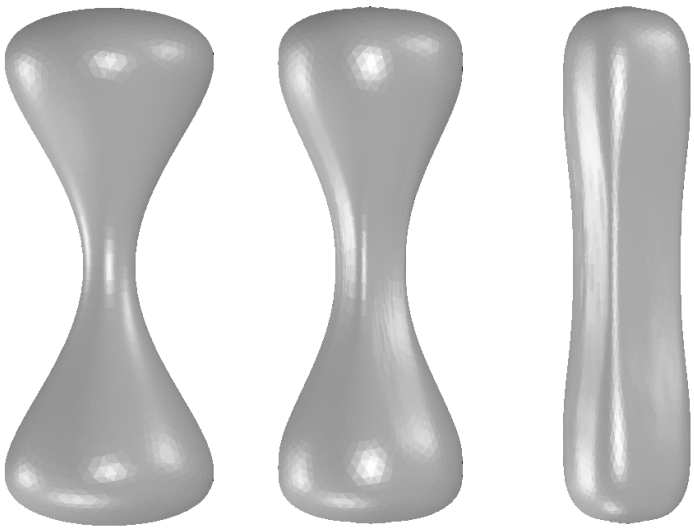

Fig. 5. From left to right the initial surface and two evolution steps of an anisotropic mean curvature flow are depicted (graphically scaled).

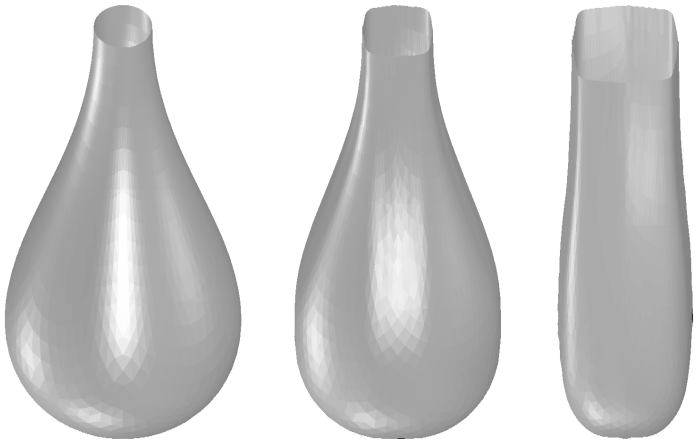

Fig. 6. The sliced surfaces of Figure 5 are shown.

The discrete normal $N^{(k)}$ is piece-wise constant and so the matrix $L^{(k)}$ and the right hand sides $C_l^{(k)}$ follow the usual setup of the stiffness matrix in a finite element code via a loop over the triangles. Only a constant factor has to be included on every triangle.

In Figure 5 and Figure 6 a result of an anisotropic evolution is shown. The anisotropy is similarly chosen as in Figure 3.

5 Curve and Surface Classification

In this section we will describe two methods for the local classification of curves and surfaces. This will enable us to distinguish smooth areas on the curve or surface from edge or corner regions. Both methods will be robust with respect to noise. Later on in Section 6 we will make use of these local classifications to process noisy curves and surfaces.

5.1 Classification via Curvature Analysis

In this approach, the quantity for the detection of edges is the curvature tensor, in case of codimension 1 represented by the symmetric shape operator $S_{\mathcal{T}_x\mathcal{M}}$ (note that we identify $x(\mathcal{M})$ and $\mathcal{M}$ and consequently x and ξ). An edge is supposed to be indicated by one sufficiently large eigenvalue of $S_{\mathcal{T}_x\mathcal{M}}$.

We define a tensor depending on $S_{\mathcal{T}_x\mathcal{M}}$, which considered as diffusion tensor (see Section 6.1) enables us to decrease diffusion significantly at edges indicated by $S_{\mathcal{T}_x\mathcal{M}}$. This tensor locally classifies the curve or surface.

Furthermore we will introduce a threshold parameter λ (see equation (19)) for the identification of edges. Roughly speaking, this parameter enables us to define what is an important characteristic.

The evaluation of the shape operator on a noisy surface might be misleading with respect to the original but unknown surface and its edges. Thus we prefilter the surface $\mathcal{M}$ before we evaluate the shape operator. The straightforward "geometric Gaussian" filter is a short time-step $\tau = \sigma^2/2$ of mean curvature motion. Hence, we compute a shape operator $S_{\mathcal{T}_x\mathcal{M}_\sigma}$ on the resulting prefiltered surface $\mathcal{M}_\sigma$. Here the parameter σ is the "geometric Gaussian" filterwidth.

For every point x on $\mathcal{M}_\sigma$ the tensor $a^\sigma_{\mathcal{T}_x\mathcal{M}_\sigma}$ is supposed to be a symmetric, positive definite, linear mapping on the tangent space $\mathcal{T}_x\mathcal{M}_\sigma$:

$$a^\sigma_{\mathcal{T}_x\mathcal{M}_\sigma}(x) : \mathcal{T}_x\mathcal{M}_\sigma \to \mathcal{T}_x\mathcal{M}_\sigma \ .$$

There is an orthonormal basis $\{w^{1,\sigma}, w^{2,\sigma}\}$ of $\mathcal{T}_x\mathcal{M}_\sigma$ such that $S_{\mathcal{T}_x\mathcal{M}_\sigma}$ is represented by

$$S_{\mathcal{T}_x\mathcal{M}_\sigma} = \begin{pmatrix} \kappa^{1,\sigma} & 0 \\ 0 & \kappa^{2,\sigma} \end{pmatrix} \tag{18}$$

because of the symmetry of the shape operator. Now we consider a tensor which is defined with respect to the above orthonormal basis as follows:

$$a^\sigma_{\mathcal{T}_x\mathcal{M}_\sigma} = \begin{pmatrix} G\left(\frac{\kappa^{1,\sigma}}{\lambda}\right) & 0 \\ 0 & G\left(\frac{\kappa^{2,\sigma}}{\lambda}\right) \end{pmatrix} \tag{19}$$

with the function G as defined in the introduction.

Hence, due to the anisotropy defined in (19), a point belongs to an edge if there is a principal direction of curvature on $\mathcal{M}_\sigma$ with large curvature compared to λ. If the second principal curvature is small w.r.t. λ, we regard the first direction as orthogonal to an edge on the surface. At corners both principal curvatures of $\mathcal{M}_\sigma$ are large.

In summary, analyzing our classification tensor leads to a surface classification as follows: Smooth parts of the surface can be characterized by $a^\sigma_{\mathcal{T}_x\mathcal{M}_\sigma} \backsim \mathrm{diag}[1,1]$. An edge can be defined via the relation $a^\sigma_{\mathcal{T}_x\mathcal{M}_\sigma} \backsim \mathrm{diag}[1,0]$. In this case, the direction along the edge is given by $w^{2,\sigma}$ where we assume here $|\kappa^{1,\sigma}| >> |\kappa^{2,\sigma}|$. In this setting, corners are given by the relation $a^\sigma_{\mathcal{T}_x\mathcal{M}_\sigma} \backsim \mathrm{diag}[0,0]$. We may introduce as an edge-indicator the function $\eta_\lambda(x) = \mathrm{tr}\ a^\sigma_{\mathcal{T}_x\mathcal{M}_\sigma}$. Depending on the parameter λ edges and corners are given by $\eta_\lambda < 1$.

5.2 Classification via Moments

The second approach to local surface classification is to use the zero surface moments. This allows to distinguish smooth regions from the vicinity of edges on the curve or surface. Hence, we compute for $x : \mathcal{M} \to \mathbb{R}^{d+1}$ the barycenter $M^0_\epsilon(x(\xi)), \xi \in \mathcal{M}$,

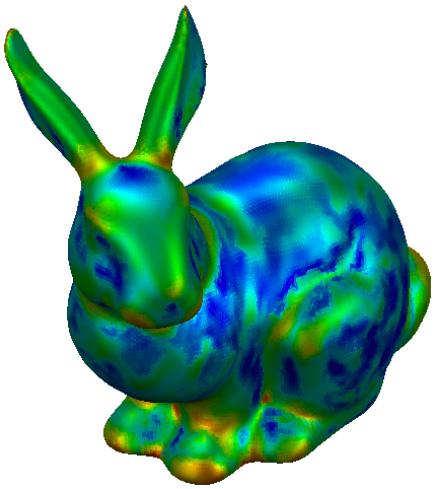

Fig. 7. The curvature classification scheme, where the trace of the classification operator is color coded. Red means that the trace is approximately 0, blue indicates smooth domains where the trace equals 2. (cf. color plate 10, Page 671)

of $x(\mathcal{M}) \cap B_\epsilon(x(\xi))$, where $B_\epsilon(x(\xi))$ is the Euclidian ϵ-ball. The parameter ϵ will be called the scanning-width.

It is well known, that the difference $n_\epsilon(\xi) = M^0_\epsilon(x(\xi)) - x(\xi)$ (denoted as the ϵ-normal) is independent of translations and in addition $|n_\epsilon(\xi)|$ is independent of rotations. We will show that a locally smooth surface is characterized by a quadratic scaling of n_ϵ in ϵ and close to edges we observe a linear scaling. Let us first consider a locally smooth curve or surface. For a smooth function η on a Euclidian ϵ-ball $B_\epsilon(0) \subset \mathbb{R}^d, d = 1, 2$, we have:

$$\begin{aligned}
\fint_{B_\epsilon} \eta &= \fint_{B_\epsilon} \eta(0) + \nabla\eta(0) \cdot x + \frac{1}{2}\nabla^2\eta(0)x \cdot x\, dx + o(\epsilon^2) \\
&= \eta(0) + \frac{1}{2}\fint_{B_\epsilon(0)} \nabla^2\eta(0)x \cdot x\, dx + o(\epsilon^2) \\
&= \eta(0) + \frac{1}{2}\lambda_i \fint_{B_\epsilon(0)} x_i^2 dx + o(\epsilon^2),
\end{aligned}$$

where each λ_i is an eigenvalue of $\nabla\eta^2(0)$. Therefore we have:

$$\begin{aligned}
\fint_{B_\epsilon} \eta &= \eta(0) + \frac{1}{2} \cdot \frac{1}{d} \fint_{B_\epsilon(0)} |x|^2 dx \cdot \operatorname{tr} \nabla^2\eta(0) + o(\epsilon^2) \\
&= \eta(0) + \frac{1}{2} \cdot \frac{1}{d} \cdot \frac{1}{4-d}\epsilon^2 \Delta\eta(0) + o(\epsilon^2).
\end{aligned}$$

In a first step we replace in our considerations the Euclidean ball $B_\epsilon(x(\xi)) \subset \mathbb{R}^{d+1}$ by a geodesic ball $\widetilde{B}_\epsilon(x(\xi)) \subset \mathcal{M}$ and compute the barycenter $\widetilde{M}^0_\epsilon(x(\xi))$ of $\widetilde{B}_\epsilon(x(\xi)) \cap$

$\mathcal{M}$. For the evaluation of $\int_{\widetilde{B}_\epsilon(x(\xi))} x(\xi) dA(\xi)$ we use normal coordinates, i.e.,

$$g_{ij}(0) = \delta_{ij} \ , \partial_k g_{ij}(0) = 0 \, .$$

Then one obtains for the Laplacian on $\mathcal{M}$ at $x(\xi)$:

$$(\Delta_{\mathcal{M}} f)(x(\xi)) = (\partial_i \partial_i f)(0) = \Delta f(0) \, ,$$

where $f \in C^2(\mathcal{M})$. For the difference $\widetilde{M}^0_\epsilon(x(\xi)) - x(\xi)$ we obtain

$$\begin{aligned}
\widetilde{M}^0_\epsilon(x(\xi)) - x(\xi) &= \fint_{B_\epsilon(0)} x dA - x(\xi) \\
&= \frac{1}{2d} \cdot \frac{1}{4-d} \epsilon^2 \Delta x(0) + o(\epsilon^2) \\
&= \frac{1}{2d} \cdot \frac{1}{4-d} \epsilon^2 \Delta_{\mathcal{M}} x(\xi) + o(\epsilon^2) \\
&= -\frac{1}{2d} \cdot \frac{1}{4-d} \epsilon^2 h(\xi) n(\xi) + o(\epsilon^2) \, ,
\end{aligned}$$

where h is the mean curvature of $\mathcal{M}$. The ratio $|\widetilde{B}_\epsilon(x(\xi))|/|B_\epsilon(x(\xi)) \cap \mathcal{M}|$ converges to 1, where $\epsilon \to 0$. So far we have shown:

Theorem 5.7 *Let $x : \mathcal{M} \to \mathbb{R}^{d+1}$, $d = 2, 3$, be an immersion. For $\xi \in \mathcal{M}$ consider a ball of radius ϵ with center $x(\xi)$ and the ϵ-normal $n_\epsilon(\xi) = M^0_\epsilon(x(\xi)) - x(\xi)$. Then n_ϵ scales quadratically in ϵ and*

$$n_\epsilon(\xi) = -\epsilon^2 \frac{1}{2d(4-d)} h(\xi) n(\xi) + o(\epsilon^2) \, .$$

Now we are going to examine the scaling w.r.t. ϵ in a non-smooth situation. Here, we restrict ourselves to curves. The generalization to surfaces in higher dimension will be subject of future work.

On account of the invariance of translation and rotation of $|M^0_\epsilon(x) - x|$ one can consider a normalized situation:

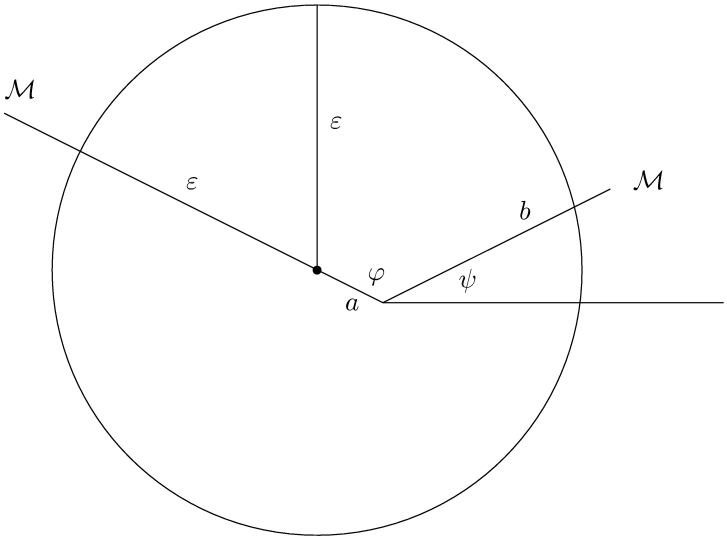

The center of the circle in the picture above is the curve-point x. For the barycenter of $\Gamma \cap B_\epsilon(x)$ we have

$$M_\epsilon^0 = \frac{(\epsilon+a)^2}{2(\epsilon+a+b)} \begin{pmatrix} -\cos\psi \\ \sin\psi \end{pmatrix} + \frac{b^2}{2(\epsilon+a+b)} \begin{pmatrix} \cos\psi \\ \sin\psi \end{pmatrix}.$$

and thus for $n_\epsilon(x)$ we obtain

$$M_\epsilon^0(x) - x = \left[\frac{(\epsilon+a)^2}{2(\epsilon+a+b)} - a \right] \begin{pmatrix} -\cos\psi \\ \sin\psi \end{pmatrix} + \frac{b^2}{2(\epsilon+a+b)} \begin{pmatrix} \cos\psi \\ \sin\psi \end{pmatrix}.$$

The length b is depending on a and φ:

$$b^2 - 2ab\cos\varphi + a^2 - \epsilon^2 = 0$$

and one computes for b:

$$b = b(\epsilon, a, \varphi) = a\cos\varphi + \sqrt{a^2\cos^2\varphi + \epsilon^2 - a^2}.$$

We now can determine $|M_\epsilon^0(x) - x|^2$ just knowing the values a, ϵ and φ:

$$\begin{aligned} & |M_\epsilon^0(x) - x|^2 \\ &= \left| \left[\frac{(\epsilon+a)^2}{2(\epsilon+a+b(\epsilon,a,\varphi))} - a \right] \begin{pmatrix} -\cos\psi \\ \sin\psi \end{pmatrix} + \frac{b^2(\epsilon,a,\varphi)}{2(\epsilon+a+b(\epsilon,a,\varphi))} \begin{pmatrix} \cos\psi \\ \sin\psi \end{pmatrix} \right|^2 \\ &= f_1^2(\epsilon,a,\varphi) + f_2^2(\epsilon,a,\varphi) + 2f_1(\epsilon,a,\varphi) f_2(\epsilon,a,\varphi)[\sin^2\psi - \cos^2\psi] \\ &= f_1^2(\epsilon,a,\varphi) + f_2^2(\epsilon,a,\varphi) + 2f_1(\epsilon,a,\varphi) \cdot \cos\varphi, \end{aligned}$$

where

$$f_1(\epsilon,a,\varphi) = \frac{(\epsilon+a)^2}{2(\epsilon+a+a\cos\varphi+\sqrt{a^2\cos^2\varphi+\epsilon^2-a^2})} - a$$

$$= \epsilon\left[\frac{\left(1+\frac{a}{\epsilon}\right)^2}{2\left(1+\frac{a}{\epsilon}+\frac{a}{\epsilon}\cos\varphi+\sqrt{\left(\frac{a}{\epsilon}\right)^2\cos^2\varphi+1-\left(\frac{a}{\epsilon}\right)^2}\right)} - \frac{a}{\epsilon}\right]$$

$$f_2(\epsilon,a,\varphi) = \frac{[a\cos\varphi+\sqrt{a^2\cos^2\varphi+\epsilon^2-a^2}]^2}{2(\epsilon+a+a\cos\varphi+\sqrt{a^2\cos^2\varphi+\epsilon^2-a^2})}$$

$$= \epsilon\frac{\left[\frac{a}{\epsilon}\cos\varphi+\sqrt{\left(\frac{a}{\epsilon}\right)^2\cos^2\varphi+1-\left(\frac{a}{\epsilon}\right)^2}\right]^2}{2\left(1+\frac{\epsilon}{a}+\frac{\epsilon}{a}\cos\varphi+\sqrt{\left(\frac{a}{\epsilon}\right)^2\cos^2\varphi+1-\left(\frac{a}{\epsilon}\right)^2}\right)}$$

Using the following definitions

$$g_1(\gamma,\varphi) = \frac{(1+\gamma)^2}{2(1+\gamma+\gamma\cos\varphi+\sqrt{\gamma^2\cos^2\varphi+1-\gamma^2}} - \gamma$$

$$g_2(\gamma,\varphi) = \frac{[\gamma\cos\varphi+\sqrt{\gamma^2\cos^2\varphi+1-\gamma^2}]^2}{1+\gamma+\gamma\cos\varphi+\sqrt{\gamma^2\cos^2\varphi+1-\gamma^2}}$$

we arrive at:

$$\left|\frac{M_\epsilon^0(x)-x}{\epsilon}\right|^2 = g_1^2\left(\frac{a}{\epsilon},\varphi\right)+g_2^2\left(\frac{a}{\epsilon},\varphi\right)+2\cos\varphi g_1\left(\frac{a}{\epsilon},\varphi\right)g_2\left(\frac{a}{\epsilon},\varphi\right) \quad (20)$$

and analyzing the local shape on two scales ϵ_1,ϵ_2 one is able to determine a and φ, the distance of x to the edge and the apex angle respectively. The rescaled ϵ-normal $\eta_\epsilon(x) := \epsilon^{-1}|n_\epsilon(x)|$ may serve as an edge indicator. If $\epsilon^{-1}|\eta_\epsilon(x)|$ exceeds a given threshold λ then we expect an edge in a neighborhood of x.

Let us point out that the above computation can be regarded as a first order approximation in case that in an edge two non-linear curve pieces intersect.

6 Applications in Curve and Surface Processing

We are now prepared to discuss the application of anisotropic curvature flow as a powerful multiscale method in curve and surface processing. Hence, we will consider two different approaches. One is based on the definition of an anisotropic diffusion tensor which incorporates the local surface classification based on the approximate shape operator. The other one takes into account the local moment analysis and derives a position dependent anisotropic surface energy integrand. In both cases the

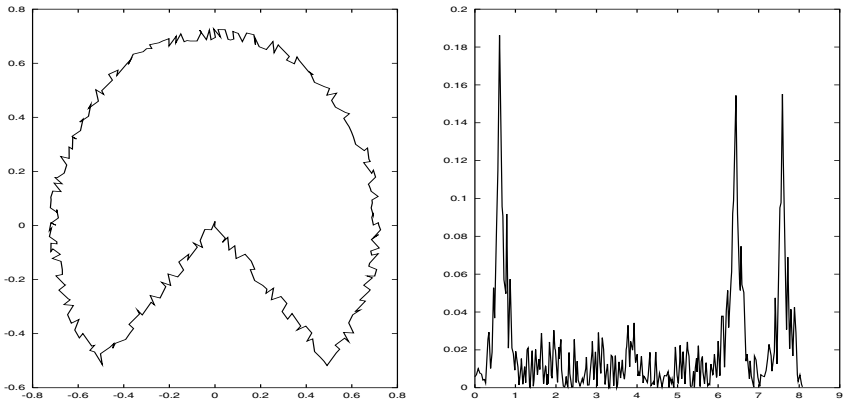

Fig. 8. Left the curve we want to analyze via moments, right the graph of $|n_\epsilon|$, where $\epsilon = 0.2$. On the abscissa of the graph the arc length is drawn; obviously three edges are clearly depicted by $|n_\epsilon|$.

solution of the resulting parabolic problem - either the diffusion problem itself or the gradient flow corresponding to the defined energy - deliver a multiscale of surface representations. For increasing time, in the evolution noise is reduced. Simultaneously features on the curves and surfaces are preserved. Let us already emphasize that especially the gradient flow approach is capable to evolve sharp edges in regions where the classification gives strong evidence for an edge feature. Thus, to our knowledge this is the first multiscale method, which not only retains features for longer times, but robustly enhances them.

We consider a noisy initial curve or surface $\mathcal{M}_0$. Both approaches share the general algorithm outline:

- A local classification is involved to figure out the expected curve or surface shape especially distinguishing between smooth areas, edges and corners (cf. Section 5).
- In time the multiscale evolution is driven by forces derived from the current local classification (cf. Section 3).

Thereby a family of surfaces $\{\mathcal{M}(t)\}_{t\in\mathbb{R}_0^+}$ is generated, where the time t serves as the scale parameter. Spatial discretization based on finite element and time-step algorithms are applied to implement the multiscale methods numerically on usual triangulated curves or surfaces (cf. Section 4). Thus, with respect to our building blocks *classification* and *evolution*, the complete algorithms cycle through the local classification and the next time step. The classification results and the curve or surface metric are always considered explicitly in every time-step.

The resulting methods lead to spatial displacement and the volume enclosed by $\mathcal{M}(t)$ is changed in the evolution. An additional force f in the evolution depending on certain integrated curvature expressions leads to volume preservation and further improves our methods.

6.1 Generalized Mean Curvature Motion in Surface Processing

We will explain how one can use the classification via curvature analysis in our general scheme. To this aim we take into account the tensor $a^{\sigma}_{\mathcal{T}_x\mathcal{M}_\sigma}$ introduced in Section 5. This tensor classifies the surface and indicates edges together with its tangential edge direction as well as corners. Now, we consider a diffusion method involving a closely related tensor $a^{\sigma}_{\mathcal{T}_x\mathcal{M}}$. We use $a^{\sigma}_{\mathcal{T}_x\mathcal{M}_\sigma}$ for its definition.

W.r.t. surface processing, our model integrates tangential smoothing along edges into the multiscale approach. To define the actual diffusion on $\mathcal{T}_x\mathcal{M}$ we decompose a vector $z \in \mathbb{R}^3$ in the orthogonal basis $\{w^{1,\sigma}, w^{2,\sigma}, N^\sigma\}$ (cf. Section 5.1), i.e.,

$$z = (z \cdot w^{1,\sigma})w^{1,\sigma} + (z \cdot w^{2,\sigma})w^{2,\sigma} + (z \cdot N^\sigma)N^\sigma$$

where $\{w^{1,\sigma}, w^{2,\sigma}\} \subset \mathbb{R}^3$ denotes the embedded tangent vectors corresponding to the basis $w^{1,\sigma}, w^{2,\sigma}$ (see equation (18)) and N^σ is the surface normal of $\mathcal{M}_\sigma$. Thus, we define the diffusion coefficient $a^{\sigma}_{\mathcal{T}_x\mathcal{M}}$ in a sloppy but intuitive way by

$$\begin{aligned} a^{\sigma}_{\mathcal{T}_x\mathcal{M}}\, z := \Pi_{\mathcal{T}_x\mathcal{M}}\Big(& G(\kappa^{1,\sigma})(z \cdot w^{1,\sigma})w^{1,\sigma} \\ & + G(\kappa^{2,\sigma})(z \cdot w^{2,\sigma})w^{2,\sigma} + (z \cdot N^\sigma)N^\sigma \Big), \end{aligned} \tag{21}$$

Here $\Pi_{\mathcal{T}_x\mathcal{M}}$ denotes the orthogonal projection onto the tangent space $\mathcal{T}_x\mathcal{M}$ and we identify the operator on the abstract tangent space and the endomorphism in $\mathbb{R}^3$.

Using $a^{\sigma}_{\mathcal{T}_x\mathcal{M}}$ as diffusion tensor ends up with the following type of parabolic surface evolution problem. Given an initial compact embedded manifold $\mathcal{M}_0$ in $\mathbb{R}^3$, we compute a one parameter family of manifolds $\{\mathcal{M}(t)\}_{t\in\mathbb{R}^+_0}$ with corresponding coordinate mappings $x(t)$ which solves the system of anisotropic geometric evolution equations:

$$\partial_t x - \operatorname{div}_{\mathcal{M}(t)}(a^{\sigma}_{\mathcal{T}_x\mathcal{M}}\, \nabla_{\mathcal{M}(t)} x) = 0 \ \text{ on } \ \mathbb{R}^+ \times \mathcal{M}(t), \tag{22}$$

and satisfies the initial condition

$$\mathcal{M}(0) = \mathcal{M}_0.$$

Hence, due to the anisotropy defined in (19), we enforce a signal enhancement in a principal direction of curvature with curvature larger than λ. If the second principal curvature is smaller than λ we regard the first direction as orthogonal to an important edge on the surface which is going to be sharpened. Simultaneously, in the other direction - the tangent direction along the edge - we invoke smoothing. At approximate corners both principal curvatures are large, thus sharpening takes place in both directions.

To avoid tangential velocity components in the evolution we project the velocity in equation (22) in normal direction and obtain

$$\partial_t x - (\operatorname{div}_{\mathcal{M}} \left(a^{\sigma}_{\mathcal{T}_x\mathcal{M}}\, \nabla_{\mathcal{M}} x\right) \cdot n)n = 0\,, \tag{23}$$

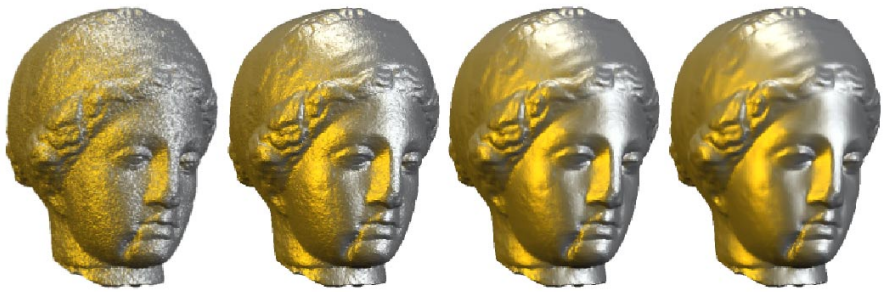

Fig. 9. *The initial surface (top left) and three timesteps from the generalized mean curvature evolution of a venus head consisting of* 268714 *triangles are shown.*

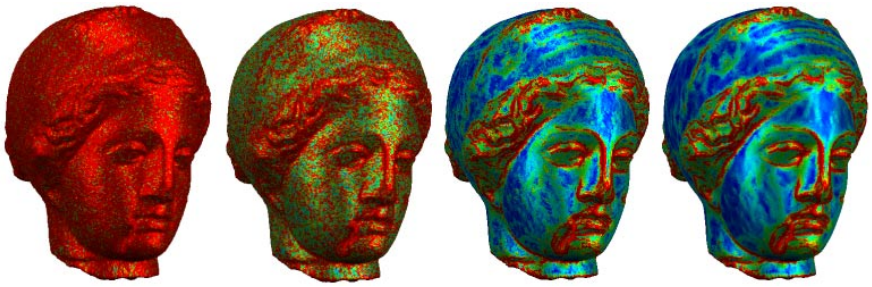

Fig. 10. *Here, for the evolution shown in Figure 9, the norm of the dominant principal curvature is color coded. (cf. color plate 9, Page 670)*

which is an example of the system (7) and indeed our diffusion method is a generalized mean curvature evolution.

In Figure 9 three time-steps of the evolution are shown. Figure 10 demonstrates that curvature is reduced significantly throughout the evolution.

6.2 A Gradient Flow Approach

We will proceed analogously as above but change the type of local classification and consider the gradient flow with respect to a surface energy.

The classification is now with respect to moments. As we saw in Section 5 we can distinguish a non-smooth situation from a smooth one by use of different scaling properties of the ϵ-normal. W.r.t. the definition of a normal velocity we want to have isotropic mean curvature evolution in smooth areas. Close to edges and corners we aim at the definition of an anisotropic mean curvature evolution respecting the local shape of the surface. This can be done by prescribing locally different Wulff-shapes.

Indeed, we consider a gradient flow for the energy (8). This implies that in $x(\xi)$ we prescribe the Wulff shape defined by $\gamma(\xi, \bullet)$.

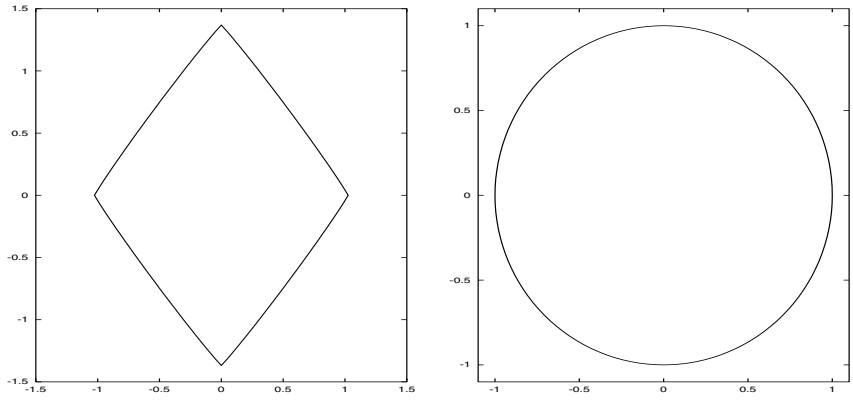

Fig. 11. Two prototypes of prescribed Wulff shapes occurring typically in the evolution steered by the gradient flow of energy (8).

If a point ξ is classified to be smooth and the distance to non-smooth domains is large enough (belonging by definition to the set $\mathcal{S}$), the local Wulff-shape is the sphere, i.e., one has the isotropic integrand $\gamma(\xi, n) = |n|$.

In the present paper we confine to the case of curves concerning the definition of γ in the remaining set $\mathcal{M} - \mathcal{S}$.

On curves, we just have to determine *edges* together with their *apex angles* and the *directions of the apex angle*. Assume that for a given scanning-width ϵ a neighborhood $\mathcal{N}_\epsilon$ of an edge is defined by

$$\mathcal{N}_\epsilon = \{x \in \mathcal{M} \,|\, \epsilon^{-1}\|n_\epsilon\| \geq \lambda\}$$

where λ is some threshold parameter. A point ξ_0, where n_ϵ achieves a local maximum in $\mathcal{N}_\epsilon$ is defined to be an edge. This is motivated by the observation that in (20) the left hand side is maximal for $a = 0$. The corresponding direction of the apex angle in $x(\xi_0)$ is given by $n_\epsilon(\xi_0)$. It remains to determine the apex angle. Using two scanning-widths ϵ and $r\epsilon$, where r is a positive constant (in our applications we choose $r = 2$), we are able to compute the apex angle by relation (20). Now we define for all $\xi \in \mathcal{N}_\epsilon$ the integrand $\gamma(\xi, n) = \gamma_0(n)$ and γ_0 determines a Wulff-shape whose apex angle and direction of apex angle coincides with the computed quantities of the curve on $\mathcal{N}_\epsilon$. Furthermore we choose γ_0 as an even integrand, i.e., $\gamma_0(n) = \gamma_0(-n)$. This enables us to treat convex and concave situations equivalently. By definition Wulff-shapes are convex bodies and on a first glance it seems to be impossible to enhance concave situations. But by the choice of even integrands it is energetic favourable to enhance a concave edge instead of convexifying the situation. Finally, we use interpolation in $\gamma(\cdot, n)$ which lead to a convex blending from the non-smooth Wulff-shape to the sphere a long the curve if we move from the neighborhood of an edge to a smooth region (see Figure 11).

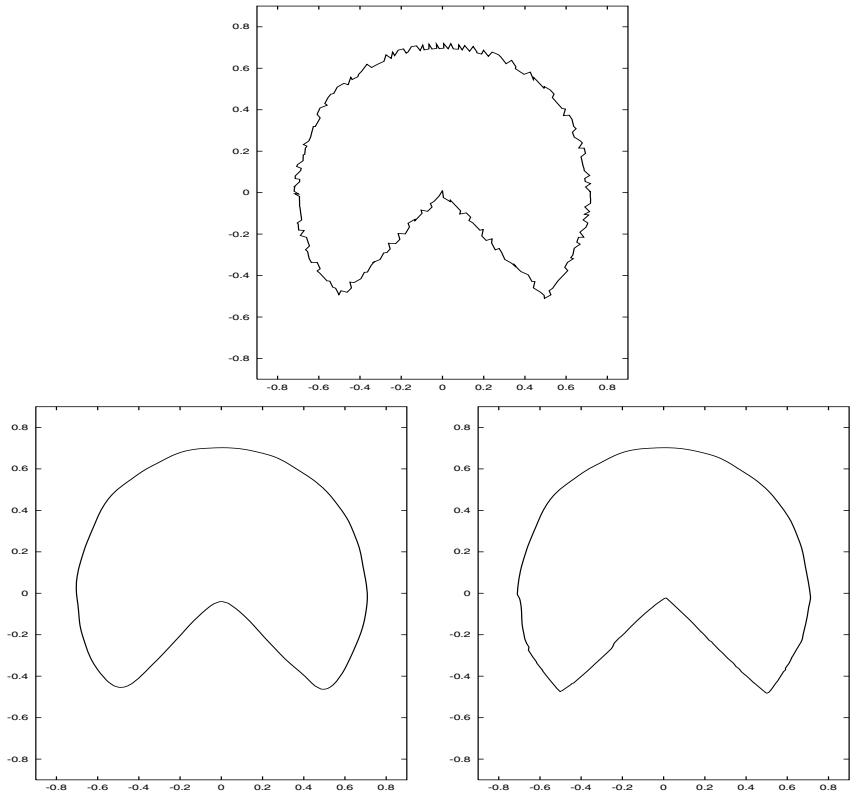

Fig. 12. On top the initial surface is depicted, bottom left a time-step of a mean curvature evolution and bottom right the same time-step is chosen for the anisotropic evolution.

Figure 12 shows a comparison between mean curvature evolution and our gradient flow approach. In Figures 13 and 14 we see results of this method.

Volume Conservation

Now we come to a theorem that allows to define an algorithm for image processing that keeps the enclosed volume fixed.

Theorem 6.8 *Let $a : \mathcal{T}_x\mathcal{M} \to \mathcal{T}_x\mathcal{M}$ be an endomorphism of the tangent-space in every point on $\mathcal{M}$. Then the enclosed volume of the surface does not change under the evolution*

$$\partial_t x - \left(div_{\mathcal{M}} \left(a^{\sigma}_{\mathcal{T}_x\mathcal{M}} \nabla_{\mathcal{M}} x\right) \cdot n\right) n = \overline{h}(t) n$$

if we choose $\overline{h}(t) := \frac{1}{\int_{\mathcal{M}(t)} dA} \int_{\mathcal{M}(t)} h_a \, dA$.

This theorem is an immediate consequence of the following

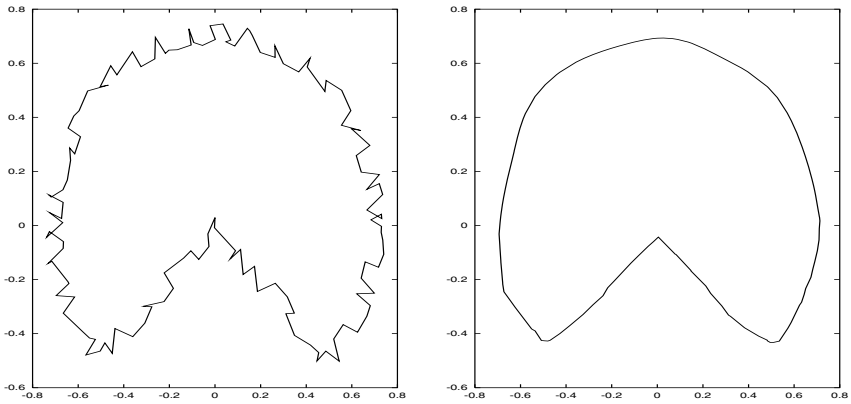

Fig. 13. The method is able to cope with strong noise. Left the initial curve is shown, right the result of the algorithm minimizing the energy (8).

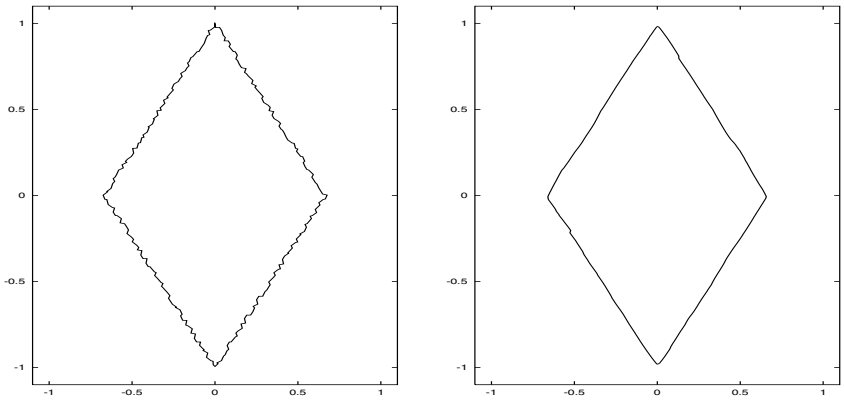

Fig. 14. This figure shows that the gradient flow method is able to handle acute and obtuse angles.

Proposition 6.9 *Consider an evolution of a surface $x(t) : \mathcal{M} \to \mathbb{R}^{d+1}$ in normal direction, i.e., $\partial_t x = \varphi\, n$. The change of the enclosed volume in time is given by*

$$\frac{d}{dt}[\mathit{Vol}(\mathcal{M}(t))]_{t=t_0} = (d+1)\int_{\mathcal{M}(t_0)} \varphi \, dA\,.$$

Proof. For the time derivative of the volume we obtain

$$\begin{aligned}
&\partial_t \int_{\mathcal{M}} (x \cdot n)\, dA \\
&= \int_{\mathcal{M}} (\partial_t x \cdot n)\, dA + \int_{\mathcal{M}} (x \cdot \partial_t n)\, dA + \int_{\mathcal{M}} (x \cdot n)\, \mathit{div}_{\mathcal{M}}(\varphi n)\, dA \\
&= \int_{\mathcal{M}} \varphi\, dA - \int_{\mathcal{M}} (x \cdot Dx(\nabla_{\mathcal{M}} \varphi)\, dA + \int_{\mathcal{M}} (x \cdot n)\, \varphi h\, dA
\end{aligned}$$

For the relations used in the above equalities see [6] and [8]. Integration by parts leads to:

$$\begin{aligned}
&\partial_t \int_{\mathcal{M}} (x \cdot n)\, dA \\
&= \int_{\mathcal{M}} \varphi\, dA + \int_{\mathcal{M}} \mathit{div}_{\mathcal{M}} x\, \varphi\, dA = (d+1) \int_{\mathcal{M}} \varphi\, dA
\end{aligned}$$

and we can finish our proof. □

Choosing φ with vanishing mean value leads to constant volume under the evolution and thus Theorem 6.8 is proved.

References

1. L. Alvarez, F. Guichard, P. L. Lions, J. M. Morel: Axioms and fundamental equations of image processing. Arch. Ration. Mech. Anal., 123, 199–257, 1993
2. G. Belletini, M. Paolini: Anisotropic motion by mean curvature in the context of finsler geometry. Hokkaido Math. J., 25, 537–566, 1996
3. T. Bonnesen, W. Fenchel: Konvexe Körper. Springer, 1934
4. F. Catté, P. L. Lions, J. M. Morel, T. Coll: Image selective smoothing and edge detection by nonlinear diffusion. SIAM J. Numer. Anal., 29, 182–193, 1992
5. I. Chavel. Eigenvalues in Riemannian Geometry. Academic Press, 1984
6. U. Clarenz. Enclosure theorems for extremals of elliptic parametric functionals. Calc. Var., online publication DOI 10.1007/s005260100128, 2001
7. U. Clarenz, U. Diewald, M. Rumpf: Nonlinear anisotropic diffusion in surface processing. Proc. Visualization 2000, 397–405, 2000
8. U. Clarenz, H. von der Mosel: Compactness theorems and an isoperimetric inequality for critical points of elliptic parametric functionals. Calc. Var., 12, 85–107, 2001
9. B. Curless, M. Levoy: A volumetric method for building complex models from range images. In: Computer Graphics (SIGGRAPH '96 Proceedings), 303–312, 1996
10. K. Deckelnick, G. Dziuk: A fully discrete numerical scheme for weighted mean curvature flow. to appear in Numer. Math.
11. K. Deckelnick, G. Dziuk: Discrete anisotropic curvature flow of graphs. Math. Modelling Numer. Anal. (RAIRO), 33, 1203–1222, 1999
12. M. Desbrun, M. Meyer, P. Schroeder, A. Barr: Implicit fairing of irregular meshes using diffusion and curvature flow. In: Computer Graphics (SIGGRAPH '99 Proceedings), 317–324, 1999
13. U. Dierkes, S. Hildebrandt, A. Küster, O. Wohlrab: Minimal Surfaces. Grundlehren der Mathematischen Wissenschaften. 295. Berlin: Springer-Verlag, 1992
14. M. P. do Carmo: Riemannian Geometry. Birkhäuser, Boston–Basel–Berlin, 1993

15. G. Dziuk: An algorithm for evolutionary surfaces. Numer. Math., 58, 603–611, 1991
16. G. Dziuk: Convergence of a semi-discrete scheme for the curve shortening flow. Mathematical Models and Methods in Applied Sciences, 4(4), 589–606, 1994
17. G. Dziuk: Discrete anisotropic curve shortening flow. SIAM J. Numer. Anal., 36, 1808–1830, 1999
18. L. Evans, J. Spruck: Motion of level sets by mean curvature. J. Diff. Geom., 33(3), 635–681, 1991
19. I. Fonseca: The wulff theorem revisited. Proc. Roy. Soc. London A, 432, 125–145, 1991
20. I. Fonseca, S. Müller: A uniqueness proof for the wulff theorem. Proc. Roy. Soc. Edinb. A, 119, 125–136, 1991
21. D. Gilbarg, N. Trudinger: Elliptic partial differential equations of second order. Grundlehren der Mathematischen Wissenschaften. 224. Berlin-Heidelberg-New York: Springer-Verlag, 1992
22. I. Guskov, W. Sweldens, P. Schroeder: Multiresolution signal processing for meshes. In: Computer Graphics (SIGGRAPH '99 Proceedings), 1999
23. G. Huisken: The volume preserving mean curvature flow. J. Reine Angew. Math., 382, 35–48, 1987
24. B. Kawohl, N. Kutev: Maximum and comparison principle for one-dimensional anisotropic diffusion. Math. Ann., 311 (1), 107–123, 1998
25. R. Kimmel: Intrinsic scale space for images on surfaces: The geodesic curvature flow. Graphical Models and Image Processing, 59(5), 365–372, 1997
26. L. Kobbelt: Discrete fairing. In: Proceedings of the 7th IMA Conference on the Mathematics of Surfaces, 101–131, 1997
27. L. Kobbelt, S. Campagna, J. Vorsatz, H.-P. Seidel: Interactive multi-resolution modeling on arbitrary meshes. In: Computer Graphics (SIGGRAPH '98 Proceedings), 105–114, 1998
28. W. Lorensen, H. Cline: Marching cubes: A high resolution 3d surface construction algorithm. Computer Graphics, 21(4), 163–169, 1987
29. R. Malladi, J. Sethian: Image processing: Flows under min/max curvature and mean curvature. Graphical Models and Image Processing, 58(2), 127–141, 1996
30. E. Pauwels, P. Fiddelaers, L. Van Gool: Enhancement of planar shape through optimization of functionals for curves. IEEE Trans. Pattern Anal. Mach. Intell., 17, 1101–1105, 1995
31. P. Perona, J. Malik: Scale space and edge detection using anisotropic diffusion. In: IEEE Computer Society Workshop on Computer Vision, 1987
32. T. Preußer, M. Rumpf: A level set method for anisotropic geometric diffusion in 3D image processing. To appear in SIAM J. Appl., 2002
33. K. Räwer: Stabile Extremalen parametrischer Doppelintegrale in $\mathbb{R}^3$. Preprint SFB 256, Univ. Bonn, 321, 1993
34. G. Sapiro: Vector (self) snakes: A geometric framework for color, texture, and multiscale image segmentation. Proc. IEEE International Conference on Image Processing, 1996
35. G. Sapiro: Geometric Partial Differential Equations and Image Processing. Cambridge University Press, 2001
36. G. Taubin: A signal processing approach to fair surface design. In: Computer Graphics (SIGGRAPH '95 Proceedings), 351–358, 1995
37. J. Weickert: Foundations and applications of nonlinear anisotropic diffusion filtering. Z. Angew. Math. Mech., 76, 283–286, 1996
38. B. White: The space of m-dimensional surfaces that are stationary for a parametric elliptic functional. Indiana Univ. Math. J., 36, 567–602, 1987
39. G. Wulff: Zur Frage der Geschwindigkeit des Wachsthums und der Auflösung der Kristallflächen. Zeitschrift der Kristallographie, 34, 449–530, 1901